

# Spin-models, dynamics and criticality with atoms in tilted optical superlattices

Anton S. Buyskikh,<sup>1,\*</sup> Luca Tagliacozzo,<sup>1,2</sup> Dirk Schuricht,<sup>3</sup> Chris A. Hooley,<sup>4</sup> David Pekker,<sup>5</sup> and Andrew J. Daley<sup>1</sup>

<sup>1</sup>*Department of Physics and SUPA, University of Strathclyde, Glasgow G4 0NG, UK*

<sup>2</sup>*Departament de Física Quàntica i Astrofísica and Institut de Ciències del Cosmos (ICCUB),  
Universitat de Barcelona, Martí i Franquès 1, 08028 Barcelona, Catalonia, Spain*

<sup>3</sup>*Institute for Theoretical Physics, Center for Extreme Matter and Emergent Phenomena,  
Utrecht University, Princetonplein 5, 3584 CE Utrecht, The Netherlands*

<sup>4</sup>*SUPA, School of Physics and Astronomy, University of St Andrews, North Haugh, St Andrews KY16 9SS, UK*

<sup>5</sup>*Department of Physics and Astronomy, University of Pittsburgh, Pittsburgh, PA 15260, USA*

(Dated: November 20, 2018)

We show that atoms in tilted optical superlattices provide a platform for exploring coupled spin chains of forms that are not present in other systems. In particular, using a period-2 superlattice in 1D, we show that coupled Ising spin chains with XZ and ZZ spin coupling terms can be engineered. We use optimized tensor network techniques to explore the criticality and non-equilibrium dynamics in these models, finding a tricritical Ising point in regimes that are accessible in current experiments. These setups are ideal for studying low-entropy physics, as initial entropy is “frozen-out” in realizing the spin models.

Systems of ultracold atoms are regularly discussed and utilized as quantum simulators, to engineer models of interest from other many-body physical systems that are computationally complex and explore their properties [1–4]. However, the unique properties of these systems can also motivate the study of genuinely novel many-body physics — especially including a wide variety of phenomena in out-of-equilibrium dynamics [5–7]. In this work, we explore spin models that arise naturally for ultracold atoms loaded in an optical superlattice potential together with a gradient potential. This gives rise to spin chains with unusual couplings that are readily explorable in experiments and can exhibit interesting phenomena both in and out of equilibrium.

Previous experiments have shown long-lived coherences for dynamics of strongly interacting atoms confined to move along one dimension of a tilted optical lattice [8–11]. The origin of these coherences was investigated in Ref. [12], which considered all states resonantly coupled to that with a single atom in every lattice site, then when the energy difference along the potential gradient between neighboring lattice sites,  $E$ , is equal to the on-site interaction energy shift  $U$ , the system was mapped onto an effective skew-field Ising model. Our work is strongly motivated by experiments observing resonant dynamics for  $E = U/n$  with  $n = 1, 2, 3, \dots, 6$  [11]. However, without a superlattice potential there are more resonantly coupled states than can be represented in a spin model. Here we show that by adding a superlattice potential, it is possible to make use of these resonant dynamics to represent an unusual form of coupled Ising spin chains. We analyze the behavior of these systems using symmetry arguments and computational techniques with projected matrix product operators. We identify unusual critical behavior, which we characterize as a tricritical point in the phase diagram, and analyze characteristic quench dynamics that would be directly observable in ongoing ex-

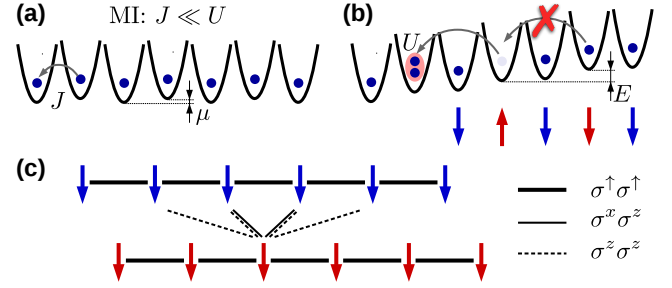


FIG. 1. Spin model example from a tilted period-2 superlattice. (a) We consider states that are near-resonantly coupled to a unit filled MI phase of bosons on a superlattice with period 2, and a superlattice energy offset between sites  $\mu$ . (b) For resonant tunnelling of atoms over two sites,  $E \approx U/2$ , the superlattice provides a closed spin-1/2 model, where a spin is labelled  $|\uparrow\rangle$  if the particle has tunneled by two sites, and  $|\downarrow\rangle$  if it has not tunneled. There is a strong constraint preventing two consecutive spin-up states in any sublattice, as this state is not resonantly coupled. (c) The resulting effective spin model (3) can be represented as two separate Ising spin chains, one for each sublattice. As discussed in the text, this setup provides unusual couplings between these spin chains: chains of odd (blue) and even (red) spins coupled with each other via  $\sigma^x \sigma^z$  and  $\sigma^z \sigma^z$  interactions (shown only for one spin).

periments.

*Model* – The underlying description of the experiment when atoms are confined to the lowest band of a sufficiently deep 1D optical lattice is the modified Bose-Hubbard model ( $\hbar \equiv 1$ )

$$H = -J \sum_{\langle i,j \rangle} b_i^\dagger b_j + \frac{U}{2} \sum_i n_i(n_i - 1) - \sum_i V_i n_i, \quad (1)$$

where  $J$  is the tunnelling matrix element,  $\langle \cdot, \cdot \rangle$  implies summation only over neighboring sites, and  $V_i = E \cdot i + (-1)^i \cdot \mu/2$  is the linear energy shift with the superlattice

energy offset  $\mu$ .

By loading atoms into a deep lattice with  $U \gg J$ , we can always begin from a unit filled Mott Insulator (MI) state with atoms exponentially localized at individual lattice sites. When the tilt is tuned to the vicinity of a resonance  $E = U/n$ ,  $n = 1, 2, 3, \dots$  long-range resonantly enhanced tunnelings of  $n^{\text{th}}$  order become possible on the experimental time scales [9–11]. These studies were initially motivated by theoretical work for  $n = 1$  by Sachdev et al. [12], who proposed a mapping between spatial degrees of freedom of bosons and effective spins. Each boson that stays on its initial site of the parent MI state is mapped with a spin down  $|\downarrow\rangle$  and each boson that resonantly hops to the first neighboring site as a spin up  $|\uparrow\rangle$ .

In the regime  $|U - E|, J \ll E, U$  the behavior of bosons at relevant time scales can then be mapped to the effective model

$$H_U = \sum_i \left[ -\sqrt{2}\sigma_i^x + \lambda\sigma_i^\uparrow + W\sigma_i^\uparrow\sigma_{i+1}^\uparrow \right], \quad (2)$$

where  $\lambda = (U - E)/J$  denotes the deviation from the resonance,  $\sigma^\uparrow = (\sigma^z + 1)/2$  is a projector on the spin-up state, and  $W \rightarrow +\infty$  is the constraint preventing two consecutive spin-ups, as this configuration would not be resonantly coupled and has occupation suppressed  $\propto (J/U)^2$ . In later works non-equilibrium dynamical properties [13] and high order corrections [14] were investigated within this model. The model (2) is referred as the antiferromagnetic Ising chain in a skew field (AFISF), which exhibits two phases: an ordered AFM phase and paramagnetic (PM) phase with spins aligned with the skew field [15]. These two phases are separated by a second order phase transition line on the plane of both transverse and parallel fields, reflecting the breaking of a  $\mathcal{Z}_2$  symmetry.

*Spin model for  $n = 2$*  – When we consider  $n > 1$ , we will naturally be considering higher-order tunnelling processes. We note that there was direct experimental verification of second and third order tunnelling in the small parameter  $J/E \sim J/(U/n)$  in Ref. [11]. As a result, it is necessary to employ the superlattice potential, as second order tunnelling processes without the superlattice would already give rise to atom configurations that are not describable by the spin half model defined for the  $n = 1$  case. In the presence of a superlattice, we can produce a spin model by considering each sublattice (separating the even sites and odd sites) for  $n = 2$ , and defining the spin model similarly to the  $n = 1$  case, but based on tunnelling within each sublattice, as depicted in Fig. 1.

Using this mapping in the regime  $|U/2 - E|, J \ll \mu \ll E, U$  we obtain the effective Hamiltonian of the following

form, as depicted in Fig. 1(c),

$$H_{U/2} = \sum_i \left[ -\sqrt{2}\sigma_i^x + \lambda\sigma_i^\uparrow + W\sigma_i^\uparrow\sigma_{i+2}^\uparrow + \frac{8 - 56\sigma_i^\uparrow}{15} - 2\sqrt{2}(\sigma_i^x\sigma_{i+1}^z + \sigma_i^z\sigma_{i+1}^x) - \frac{8}{5}(\sigma_i^z\sigma_{i+1}^z + \sigma_i^z\sigma_{i+3}^z) \right]. \quad (3)$$

Here,  $\lambda \equiv \frac{U/2 - E}{J^2/(U/2)}$  denotes the deviation from the resonance and  $W \rightarrow +\infty$  is the constraint that forbids states with  $|\uparrow\rangle_i |\uparrow\rangle_{i+2}$ , i.e., two neighboring atoms within a sublattice cannot both tunnel, analogously to the  $n = 1$  case (with maximum occupation of the states we project out scaling as  $\propto (J/U)^4$ ). The first three terms alone are identical to (2) for each sublattice, providing two Ising subchains. The fourth term just shifts the entire energy spectrum along the energy and detuning  $\lambda$  axes due to interactions between even and odd spins.

The remaining terms result from coupling between these subchains in second order perturbation theory, and can be understood intuitively as follows. Firstly, the terms proportional to  $\sigma^x\sigma^z$  arise because as atoms tunnel within each sublattice (represented by  $\sigma^x$ ) the denominator of the resulting amplitude in second order perturbation theory will change sign depending on whether an atom is present on the intermediate site from the other sublattice (giving a  $\sigma^z$  on the neighboring site). The  $\sigma^z\sigma^z$  terms arise due to virtual energy shifts in second-order perturbation theory that are dependent on the occupation number of atoms in given sites. These can be separated by up to three sites in the spin model, because an atom can tunnel over two sites and encounter a shift depending on whether an atom is present on the neighboring (third) site. The details of the derivation are presented in Ref. [16].

Despite the relatively simple couplings, we are not aware of any other physical realization of this type of spin model. We analyzed its properties through analytical arguments and numerical calculations based on Matrix Product State and Operators (MPS/MPO) techniques [17], with all states converged in a matrix product bond dimension  $D$ . We implemented the constraint in (3) exactly with matrix product projection operators, as detailed in our accompanying paper, Ref. [16]. Finite temperature and out of equilibrium calculations were performed using a combination of Time-Dependent Variational Principle (TDVP) methods [18–21] and purification techniques [22, 23].

*Phase diagram and critical behavior* – The essential points of the phase diagram become clear if we first discuss the extreme cases. As in the  $n = 1$  case, for  $\lambda \rightarrow +\infty$  the ground state of the system is non-degenerate PM state  $\prod_i |\downarrow\rangle_i$  where spins are aligned with the strong external field  $\lambda$ , in the bosonic language the energy is minimized if all bosons stay on their initial sites of the parent MI state. In the case of  $\lambda \rightarrow -\infty$  spins in the ground state are ordered in the AFM fashion  $|\downarrow\uparrow\downarrow\rangle$ , where odd

and even spins are Neel ordered due to the constraint.

The lowest elementary excitations are single spin flips  $|j\rangle = |\uparrow\rangle_j \prod_{i \neq j} |\downarrow\rangle_i$  for the PM and domain walls for the AFM, with the energy gap over the ground state scaling as  $\sim \lambda$  in both cases. Coupling between the chains, however, lead to bound excitations on the two subchains, and this is enough to suppress the original phase transition of elementary excitations at  $\lambda = -1.85$  and create a new phase transition point, which can be seen in Fig. 2(a).

The low-energy physics of (3) is very sensitive to the precise location of the critical point  $\lambda_{\text{crit}}$  rendering the identification of the universality class of the transition very challenging [16]. We thus use a technique that, similarly to Binder cumulants [24], makes it possible to locate the critical point without any previous knowledge of the critical exponents beside assuming that the theory becomes conformally invariant. In this way we can use a prediction from conformal field theory (CFT) regarding the scaling of the entanglement entropy. For blocks of contiguous  $M$  spins embedded in a chain with periodic boundary conditions, we expect [25–28]

$$S_{\text{vN}}(M) = \frac{c}{3} \log_2 M + A + \dots, \quad (4)$$

where  $c$  is the central charge of the corresponding CFT [29–31],  $A$  is a non-universal constant and the dots suggest the possible presence of further sub-leading corrections [32–36].

We can then extract the central charge at the critical point by plotting

$$c_M = 3 \frac{S_{\text{vN}}(M) - S_{\text{vN}}(M_{\text{max}})}{\log_2(M/M_{\text{max}})}, \quad (5)$$

for several system sizes  $M$  as a function of  $\lambda$  up to  $M = 60$  in Fig. 2(b) [38]. All system sizes  $M$  considered here are chosen to be divisible by 4, which is equal to the periodicity of the AFM phase. This ensures that the ground states have the same degeneracy and hence corrections related to different degeneracies can be neglected.

At the Quantum Critical Point (QCP) the value of the function  $c_M$  i) becomes independent of  $M$  and ii) matches the value of the central charge  $c$ . In order to locate the critical point  $\lambda_{\text{crit}}$  we perform the following analysis. For each pair of lines  $c_M$  and  $c_{M+4}$  we find the intersection point  $(M_x, \lambda_x)$ , where  $M_x = M + 2$ . In Fig. 2(b) we show that  $\lambda_x(M_x)$  approach a stationary value that gives the best estimate for the critical point  $\lambda_{\text{crit}} \approx -6.6676(1)$ . The maximal discrepancy in  $\lambda_x$  between MPS bond dimensions  $D = 384$  and  $512$  is  $2 \cdot 10^{-5}$ , which does not significantly contribute to this error estimate. From Fig. 2(b) we estimate the central charge  $c \approx 0.75$ , however the presence of sub-leading correction in  $S_{\text{vN}}$  smears out the crossing points.

Since we can clearly determine that the value of the central charge is below unity, its value should match at

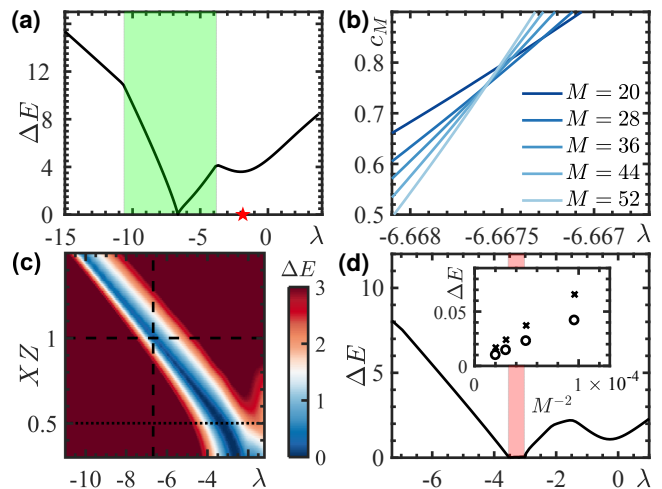


FIG. 2. (a) Energy gap  $\Delta E$  as a function of the field  $\lambda$  of Eq. (3). We choose OBC and  $M = 142$  spins such that the system always has a non-degenerate ground state in AFM and PM phases. This energy gap scaling example shows that the nature of the lowest excitations changes drastically near the QCP. Outside of the shaded green area the gap behavior is described by elementary excitations identical for the regime  $E = U$  [12]. Inside the interval the gap scales as  $\sim 2\lambda$  as bound excitation pairs have lower energy than elementary excitations. The red star denotes the QCP position in the regime  $E = U$  [12] for comparison. (b) The central charge sequence (5) near the critical point of the spin model (3) with PBC for a selection of system sizes  $M$ . The intersection points  $\lambda_x(M_x)$  converge to  $\lambda_{\text{crit}} \approx -6.6676(1)$  (see the main text). The maximal discrepancy in  $\lambda_x$  between MPS bond dimensions  $D = 384$  and  $512$  is  $2 \cdot 10^{-5}$ . (c) Energy difference between the ground and first excited states as a function of  $\lambda$  and the relative strength of  $\sigma^x \sigma^z$  interactions of Eq. (3) for OBC and  $M = 102$  spins. The position of the tricritical point is marked as the intersection of dashed lines. (d) The same as (a) but with  $XZ = 1/2$  (dotted line in (c)). The red shaded area highlights the new phase area. The inset shows scaling of the gap for two distinctly different points. Calculations were performed using DMRG and eMPS methods [37], numerical convergence was achieved for bond dimensions not larger than  $D = 512$ . The restricted spin configurations were excluded from the calculations via an MPO projector (see Appendix of [16]).

least one tabulated value of a unitary representation of the Virasoro algebra [39–42]. The two closest values of the central charge that correspond to a minimal model are  $c = 7/10$  (tricritical Ising point) and  $c = 4/5$  (3-state Potts model). We observe an extreme sensitivity of the central charge value to the critical point location. From Fig. 2(b) we see that the dependence of  $c_M$  on  $\lambda$  becomes extremely steep at the critical point as  $M$  increases. For instance, the estimated error of the critical point is  $10^{-4}$ , which in case of the largest system size  $M = 52$  leads to the central charge uncertainty  $c_M \approx 0.7 - 0.8$ . This phenomenon of high sensitivity is absent at a standard critical point (such as in the 3-state Potts model), and

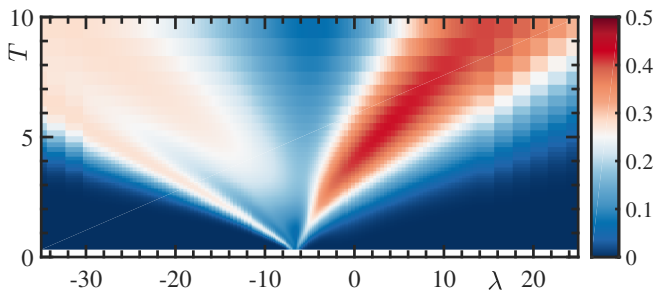


FIG. 3. Specific heat capacity per spin (6) for the system (3) of  $M = 102$  spins with open boundary conditions. Two types of excitation observed in Fig. 2(a) both approach the ground state energy. Coupled excitations correctly converge to  $\lambda_{\text{crit}}$ , which can be seen here as converging specific heat branches. Elementary excitations on the other hand always have a finite gap and their branches vanish at finite temperatures. Due to the closeness of both transitions two of four branches overlap. The results are obtained via imaginary time evolution of the infinite- $T$  density matrix via TDVP method with MPS [21] with bond dimension  $D = 128$ .

has already been observed in the context of the tricritical Ising point [36]. Furthermore, at a tricritical point three distinct phases merge and there are two relevant symmetry breaking fields. We thus expect that if the system is tricritical our  $\lambda$  is actually tuning two relevant parameters.

In order to understand the existence of a tricritical point in this model, we investigated the energy gap while adjusting the  $XZ$  parameter (Fig. 2(c,d)) representing the *relative* strength of  $\sigma^x\sigma^z$  interactions, i.e. the regime with  $XZ = 1$  is identical to the Hamiltonian (3). There we see a region appear where for a range of  $\lambda$  values the energy gap between two lowest eigenstates scales to zero with increasing system size. This suggests the existence of a third phase in the model. We conjecture that with the weakened  $\sigma^x\sigma^z$  interactions, the ground state of the new phase becomes either highly degenerate, a gapless phase of bound excitations or a floating incommensurate phase [43, 44], which would be an interesting direction for future investigations.

*Specific heat* – To connect more closely with how this might be observed in experiments, using MPO techniques to compute the finite-temperature behavior of the system, we determine the specific heat capacity per spin

$$c(T, \lambda) = \langle \Delta H_{U/2}^2(\lambda) \rangle_T / T^2 M. \quad (6)$$

Here  $\langle \Delta H^2 \rangle_T$  is the total energy variance at temperature  $T$ , and shows spectral lines that would be accessible in experiments, e.g., in spectroscopy via modulation of external fields. As shown in Fig. 3, this is significantly more complicated than we would expect for an Ising critical point. The dependence of the specific heat can be understood with a help of the energy gap in Fig. 2(a), where we see two transition points: the quantum phase transition

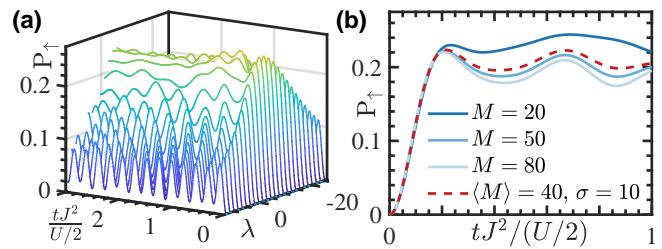


FIG. 4. Time-dependence of the average number of up-spins  $P_{\uparrow} = \sum_i \langle \sigma_i^{\uparrow} \rangle / M$ , which maps onto double occupied sites  $N_d$ , after instantaneous global quenches from the parent unit filled MI state to the regime  $E = U/2$  (3). (a) A collection of quenches with different detuning  $\lambda$  for  $M = 50$  spins and open boundaries. (b) Results of the time evolution at  $\lambda = 0$  for spin chains of length  $M$  (solid lines) and for an ensemble of spin chains, the lengths of which are normally distributed with the mean length  $\langle M \rangle = 40$  and standard deviation  $\sigma = 10$  (dashed line). Calculations were performed using the time dependent variational principle method with MPS [18–21] of converged bond dimension  $D = 128$ .

of bounded excitations, and avoided transition due to elementary excitations (used to be the phase transition of (2)). Each transition has two branches of specific heat maxima diverging from it due to thermal fluctuations. We expect that Fig. 3 actually contains four branches, but for positive  $\lambda$ , two partly overlap and cannot be distinguished.

*Quench dynamics* – Finally, we investigate dynamics of the quench from a unit filling Mott Insulator to a point near the  $E = U/2$  resonance. We see resonant behavior in the number of up-spins, centred on  $E = U/2$ , rather than the QCP itself, in analogy with dynamics at the  $E = U$  resonance [10, 45]. We also see clearly a suppression of density oscillations, in contrast to what is seen at the  $E = U$  resonance [11]. This occurs primarily because the  $\sigma^z\sigma^z$  coupling between our two chains results in a large number of frequency components in the dynamics, separated by small values of the order of the  $\sigma^x$  terms in the individual chains. This large number of frequency scales leads to this overdamping of oscillations in the number of spin-ups (observable in experiments as the number of doubly occupied sites). We note that the results of the quench dynamics in the spin system (Fig. 4) in saturation timescale and mean saturation number of doublons closely resemble the experimental results in the regime  $E = U/2$  without a superlattice [11]. This indicates that the underlying physics may be related, even though the models are different, and these connections could be more closely explored in future experiments.

*Summary and outlook* – In summary, we have shown that atoms in tilted superlattices provide a new opportunity to realize coupled spin models based on the atom number. Though we have presented a detailed analysis for bosons at an  $E = U/2$  resonance here, this work opens avenues for extensions to large numbers of coupled

chains with longer period superlattices, to 2D [46, 47], or to tunnelling of spinful fermions and bosons. Adding explicit spin species to the particles (e.g., using two atomic species or two internal states) provides a separate spin degree of freedom, and the possibility of higher-order spin models (e.g., by beginning from a spin-Mott state in the two species with one particle of each species on each site, and associating different spin states depending on which species resonantly tunnels through the lattice). The optimized tensor network techniques used here, which are detailed in Ref. [16] (together with additional analysis of the critical behavior of our model) are also applicable to a wide range of systems.

We thank Pasquale Calabrese, Florian Meinert, Manfred Mark, Giuseppe Mussardo, Roger Mong, Hanns-Christoph Nägerl, Subir Sachdev, and Jon Simon for helpful and simulating discussions. Work at the University of Strathclyde was supported by the EPSRC Programme Grant DesOEQ (EP/P009565/1), by the European Union Horizon 2020 collaborative project QuProCS - Quantum Probes for Complex Systems (grant agreement 641277), and by the EOARD via AFOSR grant number FA2386-14-1-5003. D.S. acknowledges support of the D-ITP consortium, a program of the Netherlands Organisation for Scientific Research (NWO) that is funded by the Dutch Ministry of Education, Culture, and Science (OCW). D.P. was supported by the Charles E Kaufman foundation. Results were obtained using the EPSRC funded ARCHIE-WeSt High Performance Computer (EP/K000586/1).

---

\* [anton.buyskikh@strath.ac.uk](mailto:anton.buyskikh@strath.ac.uk)

- [1] I. Bloch, J. Dalibard, and S. Nascimbène, *Nat. Phys.* **8**, 267 (2012).
- [2] M. Lewenstein, A. Sanpera, and V. Ahufinger, *Ultracold Atoms in Optical Lattices: Simulating quantum many-body systems* (OUP Oxford, 2012).
- [3] D. Jaksch and P. Zoller, *Annals of Physics* **315**, 52 (2005).
- [4] D. Jaksch, C. Bruder, J. I. Cirac, C. W. Gardiner, and P. Zoller, *Phys. Rev. Lett.* **81**, 3108 (1998).
- [5] A. Polkovnikov, K. Sengupta, A. Silva, and M. Vengalattore, *Rev. Mod. Phys.* **83**, 863 (2011).
- [6] A. J. Daley, M. Rigol, and D. S. Weiss, *New Journal of Physics* **16**, 095006.
- [7] M. Müller, S. Diehl, G. Pupillo, and P. Zoller, *Advances In Atomic, Molecular, and Optical Physics* **61**, 1 (2012).
- [8] M. Greiner, O. Mandel, T. Esslinger, T. W. Hänsch, and I. Bloch, *Nature* **415**, 39 (2002).
- [9] J. Simon, W. S. Bakr, R. Ma, M. E. Tai, P. M. Preiss, and M. Greiner, *Nature* **472**, 307 (2011).
- [10] F. Meinert, M. J. Mark, E. Kirilov, K. Lauber, P. Weinmann, A. J. Daley, and H.-C. Nägerl, *Phys. Rev. Lett.* **111**, 053003 (2013).
- [11] F. Meinert, M. J. Mark, E. Kirilov, K. Lauber, P. Weinmann, M. Gröbner, A. J. Daley, and H.-C. Nägerl, *Science* **344**, 1259 (2014).
- [12] S. Sachdev, K. Sengupta, and S. M. Girvin, *Phys. Rev. B* **66**, 075128 (2002).
- [13] M. Kolodrubetz, D. Pekker, B. K. Clark, and K. Sengupta, *Phys. Rev. B* **85**, 100505 (2012).
- [14] M. H. Muñoz Arias, J. Madroñero, and C. A. Parramurillo, *Phys. Rev. A* **93**, 043603 (2016).
- [15] A. A. Ovchinnikov, D. V. Dmitriev, V. Y. Krivnov, and V. O. Cheranovskii, *Phys. Rev. B* **68**, 214406 (2003).
- [16] A. S. Buyskikh, L. Tagliacozzo, D. Schuricht, C. A. Hooley, D. Pekker, and A. J. Daley, In preparation, to be submitted to *Phys. Rev. A* (2018).
- [17] U. Schollwoeck, *Annals of Physics* **326**, 96 (2011).
- [18] J. Haegeman, J. I. Cirac, T. J. Osborne, I. Pižorn, H. Verschelde, and F. Verstraete, *Phys. Rev. Lett.* **107**, 070601 (2011).
- [19] T. Koffel, M. Lewenstein, and L. Tagliacozzo, *Phys. Rev. Lett.* **109**, 267203 (2012).
- [20] J. Haegeman, T. J. Osborne, and F. Verstraete, *Phys. Rev. B* **88**, 075133 (2013).
- [21] J. Haegeman, C. Lubich, I. Oseledets, B. Vandereycken, and F. Verstraete, *Phys. Rev. B* **94**, 165116 (2016).
- [22] F. Verstraete, J. J. García-Ripoll, and J. I. Cirac, *Phys. Rev. Lett.* **93**, 207204 (2004).
- [23] G. D. las Cuevas, N. Schuch, D. Pérez-García, and J. I. Cirac, *New J. Phys.* **15**, 123021 (2013).
- [24] K. Binder, *Z. Physik B - Condensed Matter* **43**, 119 (1981).
- [25] C. Callan and F. Wilczek, *Phys. Lett. B* **333**, 55 (1994).
- [26] T. J. Osborne and M. A. Nielsen, *Phys. Rev. A* **66**, 032110 (2002).
- [27] G. Vidal, J. I. Latorre, E. Rico, and A. Kitaev, *Phys. Rev. Lett.* **90**, 227902 (2003).
- [28] P. Calabrese and J. Cardy, *J. Stat. Mech. Theory Exp.* **2004**, P06002 (2004).
- [29] I. Affleck, *Phys. Rev. Lett.* **56**, 746 (1986).
- [30] H. W. J. Blöte, J. L. Cardy, and M. P. Nightingale, *Phys. Rev. Lett.* **56**, 742 (1986).
- [31] J. Cardy, *J. Stat. Mech.* **2010**, P10004 (2010).
- [32] N. Laflorencie, E. S. Sørensen, M.-S. Chang, and I. Affleck, *Phys. Rev. Lett.* **96**, 100603 (2006).
- [33] P. Calabrese, M. Campostrini, F. Essler, and B. Nienhuis, *Phys. Rev. Lett.* **104**, 095701 (2010).
- [34] P. Calabrese and F. H. L. Essler, *J. Stat. Mech.* **2010**, P08029 (2010).
- [35] J. Cardy and P. Calabrese, *J. Stat. Mech. Theory Exp.* **2010**, P04023 (2010).
- [36] J. C. Xavier and F. C. Alcaraz, *Phys. Rev. B* **85**, 024418 (2012).
- [37] M. L. Wall and L. D. Carr, *New J. Phys.* **14**, 125015 (2012).
- [38] This method was initially proposed in the supplementary material of [19].
- [39] A. Belavin, A. Polyakov, and A. Zamolodchikov, *Nucl. Phys. B* **241**, 333 (1984).
- [40] M. Henkel, *Conformal Invariance and Critical Phenomena*, Theoretical and Mathematical Physics (Springer-Verlag, Berlin Heidelberg, 1999).
- [41] P. Francesco, P. Mathieu, and D. Sénéchal, *Conformal Field Theory*, Graduate Texts in Contemporary Physics (Springer-Verlag, New York, 1997).
- [42] J. L. Cardy, *Eur. Phys. J. B* **64**, 321 (2008).
- [43] P. Fendley, K. Sengupta, and S. Sachdev, *Phys. Rev. B* **69**, 075106 (2004).

- [44] N. Chepiga and F. Mila, [arXiv:1808.08990](#).
- [45] C. P. Rubbo, S. R. Manmana, B. M. Peden, M. J. Holland, and A. M. Rey, [Phys. Rev. A \*\*84\*\*, 033638 \(2011\)](#).
- [46] S. Pielawa, E. Berg, and S. Sachdev, [Phys. Rev. B \*\*86\*\*, 184435 \(2012\)](#).
- [47] A. R. Kolovsky, [Phys. Rev. A \*\*93\*\*, 033626 \(2016\)](#).